Theoretical and experimental study of quasisteady-flow separation within the glottis during phonation. Application to a modified two-mass model[a)]

X. Pelorson,[b)] A. Hirschberg, R. R. van Hassel, and A. P. J. Wijnands
Technical University of Eindhoven, W & S, Postbus 513, 5600 MB Eindhoven, The Netherlands

Y. Auregan
Laboratoire d'Acoustique de l'Université du Maine, Route de Laval, F-72000 Le Mans, France

(Received 25 August 1993; accepted for publication 14 June 1994)

Most flow models used in numerical simulation of voiced sound production rely, for the sake of simplicity, upon a certain number of assumptions. While most of these assumptions constitute reasonable first approximations, others appear more doubtful. In particular, it is implicitly assumed that the air flow through the glottal channel separates from the walls at a fixed point. Since this assumption appears quite unrealistic, and considering that the position of the separation point is an important parameter in phonation models, in this paper a revised fluid mechanical description of the air flow through the glottis is proposed, in which the separation point is allowed to move. This theoretical model, as well as the assumptions made, are validated using steady- and unsteady-flow measurements combined with flow visualizations. In order to evaluate the effective impact of the revised theory, we then present an application to a simple mechanical model of the vocal cords derived from the classical two-mass model. As expected, implementation of a moving separation point appears to be of great importance for the modeling of glottal signals. It is further shown that the numerical model coupled with a more realistic description of the vocal cord collision can lead to signals surprisingly close to those observed in real speech by inverse filtering.

PACS numbers: 43.70.Aj, 43.70.Bk

INTRODUCTION

In order to model voiced sound production both an accurate description of the vocal folds mechanical behavior and a model for the air flow through the glottis are required. Concerning the first point, important work has been done to capture the fine structure of the vocal folds and its mechanical implications.[1,2] From a fluid mechanical point of view, recent contributions either concern attempts to solve the Navier–Stokes equations numerically[3,4] or are based upon empirical considerations, pointing out, sometimes, some disagreement between the model's predictions and the experimental results.[5–7] Full numerical solutions are certainly a very important tool for a better understanding of the behavior of the flow through the vocal cords. However, due to the limits of both computation time and equipment, such an approach does not appear to be suitable for the purpose of speech production and simple models are still necessary. This paper is an attempt to provide a simple but more realistic fluid mechanical description of phonation. In particular, we propose the introduction of a moving flow-separation point during the closing phase of the oscillations of the vocal cords. The position of the flow-separation point is of particular importance for phonation since it determines not only the volume flow velocity itself but also the hydrodynamical forces exerted on the vocal folds tissues. A theory based upon a boundary-layer approximation is proposed in order to predict such an effect. The theory is validated using steady- and unsteady-flow measurements as well as unsteady-flow visualization in a simple (*in vitro*) model of the glottal channel with fixed rigid walls.

The last part of this paper is dedicated to the implementation of the flow-separation theory in a numerical model. For the sake of simplicity, we have taken what appears to be the most simple mechanical description of the vocal cords: the two-mass approximation. Unlike Ishizaka and Flanagan[8] who use a rectangular-shaped model, we propose a smooth description of the shape of the vocal cords. This representation appears to be closer to reality and also allows the introduction of a moving flow-separation point. The importance of flow separation with respect to other fluid mechanical effects is then studied on the basis of a comparison between the results obtained with the proposed model, the results obtained using a rectangular model, and glottal signals derived from inverse filtering.[9]

I. FLUID MECHANICAL DESCRIPTION OF THE FLOW THROUGH THE VOCAL CORDS, FLOW-SEPARATION EFFECTS

A. Characteristics of the vocal cords

The vocal cords can be defined as the structures including the vocal ligament (vocalis), the muscles that are attached to the ligament, and the internal part of the thyroarytenoid muscles and the mucous membrane. The narrow slit between the vocal folds is called the glottis. Typical di-

[a)]Part of this work was done while the first author was at the Institute for Perception Research (IPO).

[b)]Present address: Institut de la Communication Parlée, 46 Av. F. Viallet F-38031 Grenoble, Cedex, France.

 0001-4966/94/96(6)/3416/16/$6.00

TABLE I. Typical geometrical dimension of the vocal cords.

Length L_g	14–18 mm
Thickness d	6–9 mm
Height of the glottis h	0–3 mm

mensions observed for male speakers are presented in Table I.[10,11] These dimensions have been used in the schematic representation of the vocal cords in Fig. 1.

In the following, we will refer to the x axis as the axis parallel to the vocal cords midline, directed from the subglottal region to the vocal tract, and to the y axis as the axis perpendicular to the glottis.

B. Currently used flow models

Most flow models are based on the stationary Bernoulli equation[8,12] stating that the volume velocity U_g in the glottis is given by

$$U_g = h_{\text{out}} L_g \left(\frac{2\Delta P_{\text{Tot}}}{\rho} \right)^{1/2}, \tag{1}$$

where h_{out} is the aperture of the glottis at the end of the channel where flow separation is assumed to occur, L_g the length of the vocal cords, ρ the air density, and ΔP_{Tot} the pressure difference between the subglottal and the supraglottal region.

Several corrections are usually added to this simple formula, such as (1) pressure losses due to a vena-contracta effect, (2) viscosity effects within the glottis, (3) inertance of air, and (4) pressure recovery after the glottal outlet.

The vena-contracta effect, introduced by van den Berg *et al.*,[13] implemented numerically by Ishizaka and Flanagan[8] and recently extended by Miller,[14] refers to a flow separation, in general at the entrance of the glottis. However, such an effect is only expected to occur in the case of an abrupt contraction with sharp edges.[15] The contraction formed by the entrance of the glottis is gradual and thus it seems doubtful that any initial pressure loss would be attributable to a vena-contracta effect in such a case.

Allowance is usually made for viscosity effects within the glottis by assuming the flow to be well approximated by a bidimensional fully developed Poiseuille flow. In such a case it can be shown that

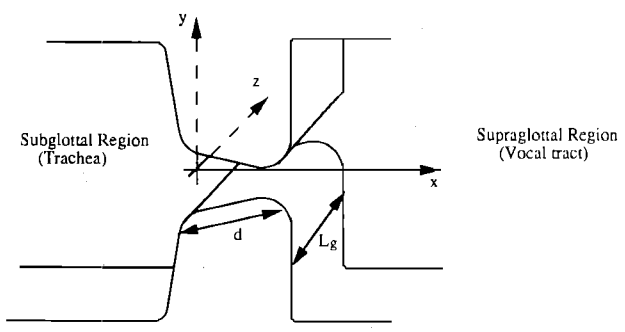

FIG. 1. Schematic representation of the vocal cords and relevant dimensions. Note that dimensions of the glottis are exaggerated.

$$\frac{dP}{dx} = -\frac{12\mu}{L_g h^3} U_g, \tag{2}$$

where μ is the dynamic viscosity coefficient, $h = h(x,t)$ the aperture of the glottis at position x, and $P = P(x)$ the pressure along the glottis. Further integration of Eq. (2) is depending on boundary conditions and thus on the geometrical description of the vocal cords used. In the usual stepwise representation the glottal shape is approximated by a succession of straight channels. For each of these channels the pressure loss due to viscosity effects is then

$$\Delta P_{\text{viscous}} = \frac{12\mu d_i}{L_g h_i^3} U_g, \tag{3}$$

where d_i is the thickness of the straight channel's element and h_i its constant height.

Inertance of air is taken into account as an additional factor $\rho(d\varphi/dt)$. Assuming an uniform flow across the glottal cross section, we have

$$\varphi = \int \frac{U_g}{hL_g}\, dx.$$

With a stepwise approximation, inertance of air induces an additional term for each elementary channel d_i, h_i:

$$\Delta P_{\text{inert}} = \frac{\rho\, d_i}{L_g} \frac{d}{dt} \left(\frac{U_g}{h_i} \right). \tag{4}$$

Finally, at the outlet of the glottis a reattachment of the flow to the vocal-tract walls is assumed. Ishizaka and Flanagan[8] proposed an evaluation of the pressure recovery by considering the quasisteady momentum-conservation equation

$$\Delta P_{\text{out}} = \frac{\rho}{2} \frac{U_g^2}{A_j^2} 2 \frac{A_j}{A_{vt}} \left(\frac{A_j}{A_{vt}} - 1 \right). \tag{5}$$

As the area of the vocal tract A_{vt} is much larger than the diameter of the jet A_j at the glottal outlet, this pressure recovery is very small.

II. A THEORETICAL PREDICTION OF FLOW SEPARATION

A. Typical flow conditions during phonation and relevant approximations

At high Reynolds numbers, the main volume-control effect is flow separation combined with turbulent dissipation of kinetic energy in the resulting jet flow. In fact, Eq. (1) implicitly assumes the formation of a free jet at the end of the glottis. In this section we consider the possibility of the formation of a free jet in the diverging part of the glottis.

The problem considered, the prediction of flow separation in a diverging channel, is of course a very general one in fluid mechanics. In the most general case this constitutes a very difficult problem that can only be solved using numerical techniques that are far too complex to be implemented within a numerical model for speech simulation. To simplify the problem, we will use in the following assumptions based

TABLE II. Typical values for the flow and oscillation frequency of the vocal cords.

Pressure difference across the glottis ΔP_{Tot}	400–2000 Pa
Mean flow velocity within the glottis u_0	10–40 m s^{-1}
Fundamental frequency of oscillation f_0	100–200 Hz
Acoustical wavelength λ_0	1.7–3.4 m

upon the consideration of typical geometrical and flow conditions observed during phonation which are summarized in Table II.

A dimensionless analysis showed that five parameters are important for this study:[16,17]

(1) The first parameter is the Strouhal number, $\mathrm{Sr}=f_0 d/u_0$. This number is a measure of the ratio of the acceleration due to the unsteadiness of the flow and the convective acceleration due to the nonuniformity of the flow. Values in Tables I and II indicate that typical Strouhal numbers are on the order of 10^{-2}. Therefore, we will assume the flow to be quasisteady in first approximation.

(2) The second parameter is the ratio of the glottal width and its length h/Lg. Since this parameter is small, we will assume the flow to be two dimensional.

(3) The Helmoltz number, the ratio of the glottal thickness and the acoustical wavelength, d/λ_0 yields information about the compactness of the flow. Since this parameter is also small, we will assume that the flow is locally incompressible.

(4) The Mach number M is the ratio of flow velocity u_0 to the speed of sound c_0. M^2 is a measure of typical density differences occurring in a steady flow. As ΔP_{Tot} is on the order of 10^{-2} times the atmospheric pressure, such compressibility effects can be considered negligible.

(5) The last parameter is the Reynolds number, $\mathrm{Re}=hU_0/\nu$. Since typical values of Re are on the order of 10^3, we will assume that the effects of viscosity can be described in terms of a boundary-layer approximation.

Of all the above assumptions, the quasisteady one is certainly the crudest but its use is justified by the simplicity of the model we are aiming at. One should also note that the viscosity effects (high Reynolds numbers approximation) can certainly no longer be neglected when the vocal cords close. The glottal aperture then becomes so narrow that viscous effects are predominant and a Poiseuille formulation similar to Eq. (2) should be considered.

B. Outline of the theory

The prediction of flow separation is of course a very general problem in fluid mechanics. However, under unsteady conditions there are very few analytical solutions and most of the time only numerical solutions are available. Because the computational time needed for these numerical resolutions is far too high for our purpose, we will restrict ourselves to a quasisteady solution for flow separation.

1. The Pohlhausen cubic method

The theoretical model proposed here is based on the boundary-layer approximation.[18,19] In other words, we consider the flow to be divided into two regions.

The first one, away from the walls, is a region where viscous effects can be neglected (main flow). In this region, the flow can be described using the usual Bernoulli equation:

$$\rho \frac{\partial \varphi}{\partial t} + P + \frac{1}{2}\rho U_0^2 = f(t), \tag{6}$$

where $U_0 = U_0(x,y)$ is the mean flow velocity, f a function of time only, and φ the potential defined by

$$\varphi = \int \mathbf{U_0}\,\mathbf{dr}.$$

The second region, the boundary layer, is a region of thickness δ, in the vicinity of the walls where the viscous effects are important and must be taken into account in the flow description. It can be shown, under the specific assumptions made (low Strouhal numbers), that the momentum equation can be reduced to the following form, also called the von Karman equation:

$$U_0^2 \frac{d\delta_2}{dx} + (2\delta_2 + \delta_1) U_0 \frac{dU_0}{dx} = \frac{\tau_0}{\rho}, \tag{7}$$

where

$$\delta_2 = \int_{\pm h/2}^{\pm(h/2-\delta)} \frac{u}{U_0}\left(1 - \frac{u}{U_0}\right) dy$$

is the momentum thickness,

$$\delta_1 = \int_{\pm h/2}^{\pm(h/2-\delta)} \left(1 - \frac{u}{U_0}\right) dy$$

is the displacement thickness,

$$\tau_0 = \mu \left(\frac{\partial u}{\partial y}\right)_{y=\pm h/2}$$

is the shear stress at the walls, and $u = u(x,y)$ is the velocity within the boundary layer.

Although Eq. (7) is already a simplification of the original momentum equation, it remains unsolvable without further assumptions since we have two unknowns, δ_1 and δ_2, and only one equation. An efficient way of solving the von Karman equation is provided by the Pohlhausen method. The key idea is to assume a given velocity profile within the boundary layer, for instance, a polynomial one:

$$\frac{u}{U_0} = \sum_{i=0}^{N} a_i \left(\frac{\eta}{\delta}\right)^i, \tag{8}$$

where η denotes the coordinate normal to the walls. Under the assumption of quasiparallel main flow used further, the coordinate η can be approximated as $\eta = h/2 - |y|$. The coefficients (a_i) of the polynomial expansion (8) for a given degree N of the polynomial are to be determined by $N+1$ boundary conditions. Unlike most textbooks which use a quartic approximation ($N=4$), we consider here a cubic ap-

proximation ($N=3$) which corresponds to the following four boundary conditions:

$$\text{at the walls } (\eta=0): \quad \begin{cases} u=0, \\ \nu\left(\dfrac{\partial^2 u}{\partial \eta^2}\right)=U_0 \dfrac{dU_0}{dx}; \end{cases}$$

$$\text{at the edge of the boundary layer } (\eta=\delta): \quad \begin{cases} u=U_0, \\ \dfrac{\partial u}{\partial \eta}=0. \end{cases}$$

With the above boundary conditions, we found the following coefficients (a_i):

$$a_0=0, \quad a_1=-\frac{1}{2}\frac{\delta^2}{\nu}\frac{dU_0}{dx}, \tag{9}$$

$$a_2=\frac{3}{2}+\frac{1}{4}\frac{\delta^2}{\nu}\frac{dU_0}{dx}, \quad a_3=-\frac{1}{2}+\frac{1}{4}\frac{\delta^2}{\nu}\frac{dU_0}{dx}.$$

With the aid of velocity profile (8) and using the above coefficients, it can be shown that the von Karman equation (7) reduces to an ordinary nonlinear differential equation,

$$\frac{dZ}{dx}=\frac{F(\lambda)}{U_0}, \tag{10}$$

with the new variables

$$Z=\frac{\delta_2^2}{\nu}$$

and

$$\lambda=Z\frac{dU_0}{dx}.$$

F is a universal function dependent only on the shape of the velocity profile and on the boundary conditions. Separation of the flow is defined as the point on the wall for which the normal derivative of the velocity is zero: $\partial u/\partial y=0$. At this point the shear stress at the walls τ_0 is also zero. With the new variable λ this occurs when $\lambda=-0.0992$. This will constitute our criterion for the prediction of flow separation.

This method was applied to several classical tests quoted by Curle[19] and was found to give much better results than other similar methods discussed by Rosenhead,[20] Curle,[19] and Blevins.[15]

2. Simplified separation prediction

Direct computation of the Pohlhausen cubic method is, of course, possible with the aid of Eq. (10). However, we experienced numerical instabilities in the vicinity of the separation point where the interaction between the boundary layer and the mean flow is important. These numerical instabilities can be avoided using specific numerical techniques such as relaxation methods or inverse techniques.[21] However, this would imply a substantial increase in computational time, which would make the method less suitable for a speech production application. For this reason, we proposed a further simplification of the method by considering the problem to be divided into two parts, as shown in Fig. 2.

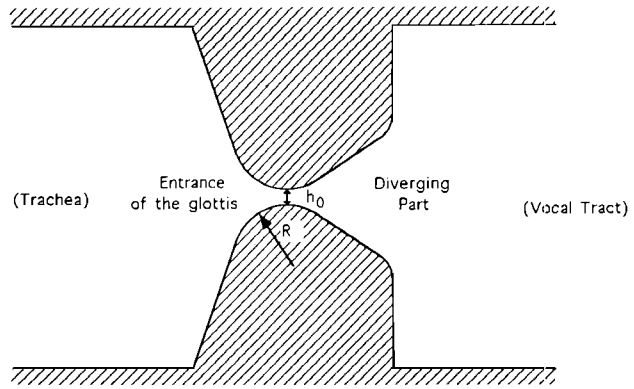

FIG. 2. Division of the channel into a converging and a diverging region.

(1) For the first region, the entrance of the channel, we consider a development of the solutions given by the Pohlhausen cubic method for a channel convergence with a constant radius of curvature R. At the minimum contraction point, in particular, it can be shown that, since the radius of curvature of the entrance R is large compared to the aperture h_0,

$$\frac{\delta_{2,0}^2}{h_0^2}=C\frac{1}{\mathrm{Re}}\left(\frac{R}{h_0}\right)^{1/2}, \tag{11}$$

where $\delta_{2,0}$ is the momentum thickness at the minimum aperture and C is a constant which has been determined numerically ($C\approx 0.015$ for $10^{-3}<h_0/R<1$).

The linear relationship (11) can of course be verified through comparison with complete numerical simulation of Eq. (10). Figure 3 shows an example of the results obtained for a wide range of R/h_0 from 1 to 1000.

(2) In the second region, the diverging part of the channel, to avoid numerical instabilities we assume that the boundary-layer growth corresponds to the Blasius solution for a flat plate in free space:[18]

$$\delta_2^2-\delta_{2,0}^2=K^2\frac{1}{\mathrm{Re}}(h-2\delta_1)x, \tag{12}$$

where $K=0.6641$.

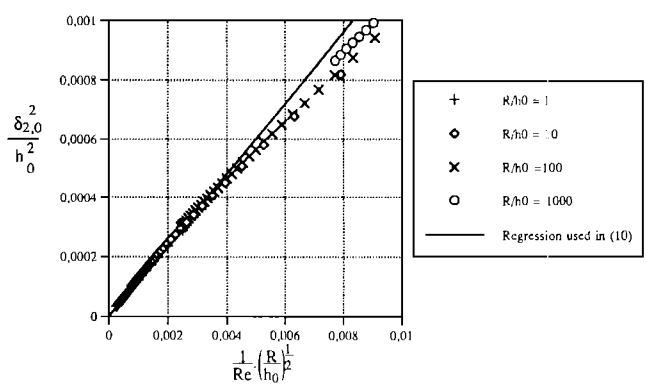

FIG. 3. Numerical computation results obtained using the Pohlhausen method for the rounded entrance of a channel. The parameter is the ratio of the minimum aperture h_0 and the radius of curvature of the channel's entrance R.

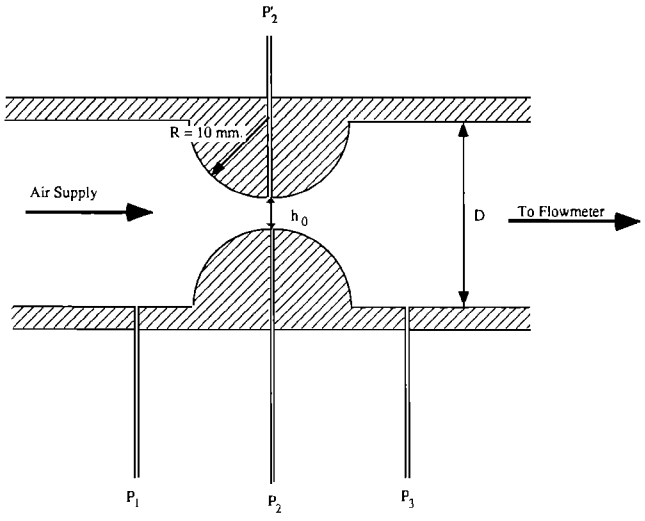

FIG. 4. Experimental setup for steady-flow measurements.

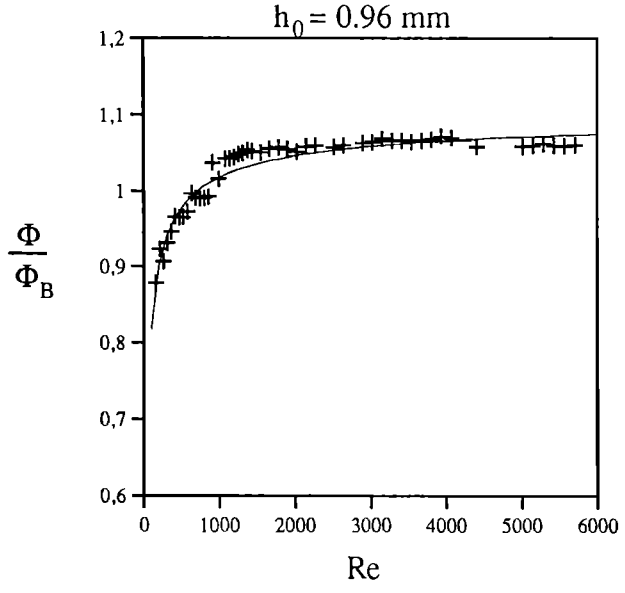

FIG. 5. Comparison between the experimental results obtained for $h_0 = 0.96$ mm and the theoretically expected results.

The criterion for flow separation can be expressed as

$$\lambda = -\delta_2^2 \,\mathrm{Re}\, \frac{1}{(h-2\delta_1)^2}\left(\frac{dh}{dx} - 2\,\frac{d\delta_1}{dx}\right) = -0.0992. \tag{13}$$

C. Experimental validation of the theory

1. Steady-flow measurements

a. Experimental setup. The experimental model is depicted in Fig. 4. It consists of a straight tube of diameter $D = 30$ mm with a contraction formed by two half-cylinders (radius of curvature $R = 10$ mm) placed perpendicular to the pipe axis. The minimum aperture of the channel h_0 (the distance between the cylinders) was a parameter that could be adjusted within 10^{-2} mm in the range of 0.1 mm $< h_0 <$ 10 mm. The dimensions used in this model were thus about three times larger than the typical physiological glottal dimensions represented in Table I.

The pressures upstream (P_1), downstream (P_3), and at the minimum contraction point (P_2 or P_2') of the model were measured using Betz micromanometers with an accuracy of ± 1 Pa. Flux measurements were obtained with the aid of calibrated rotameters. Typical accuracy was 1% for fluxes.

b. Results of the flux measurements. We will first consider the ratio of the measured flux, $\Phi = U_g/L_g$, and a reference (ideal) flux Φ_B, which we would expect for an inviscid flow with imposed separation at the minimum contraction point where $h = h_0$. With the Bernoulli relationship for the mean flow this quantity can be related to the minimum aperture, to the diameter of the jet h_s, and to the displacement thickness of the boundary layer at the separation point $\delta_{1,s}$:

$$\frac{\Phi}{\Phi_B} = \frac{h_s - 2\delta_{1,s}}{h_0}. \tag{14}$$

Figures 5 and 6 show two examples of the results obtained for a contraction of $h_0 = 0.96$ mm and $h_0 = 3.32$ mm as a function of the Reynolds number, $\mathrm{Re} = \Phi/\nu$.

Both results presented here indicate a good agreement between the theoretical prediction of Eq. (14) and the measured data over a large range of Reynolds numbers.

c. Results of the pressure drop measurements. An important quantity for the purpose of numerical simulation of the vocal cords oscillations is the ratio of the total pressure drop ΔP_{Tot} and the initial pressure drop ΔP_1. The initial pressure drop is defined as the difference between the pressure measured upstream of the contraction (P_1) and at the minimum contraction (P_2 or P_2'). By using again the Bernoulli law for the mean flow, we can show that this quantity can be expressed as

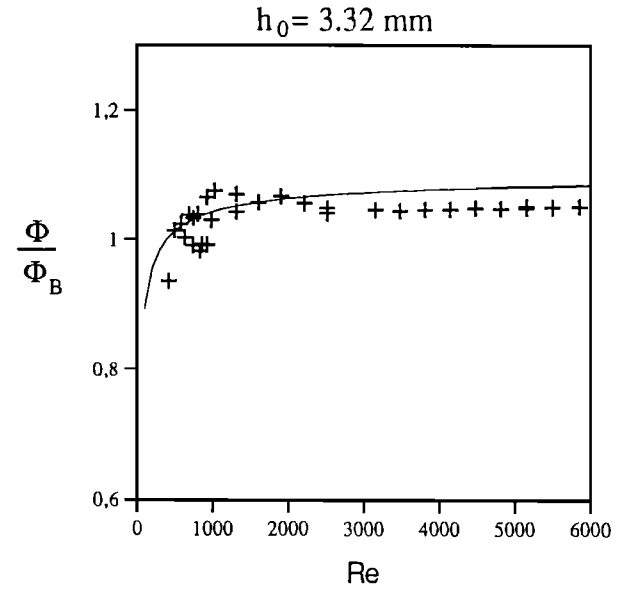

FIG. 6. Comparison between the experimental results obtained for $h_0 = 3.32$ mm and the theoretically expected results.

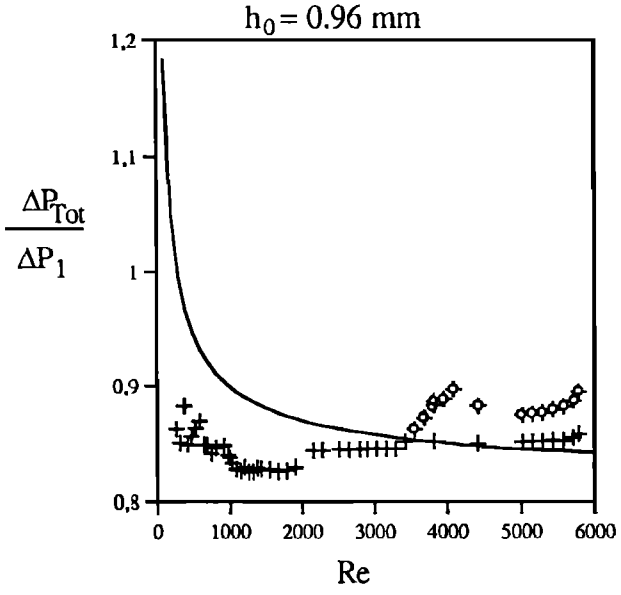

FIG. 7. Experimentally obtained and theoretically expected normalized pressure drop results for $h_0=0.96$ mm. The symbol + refers to P_2 measurements, -◇- to P_2' measurements.

$$\frac{\Delta P_{\mathrm{Tot}}}{\Delta P_1}=\frac{\dfrac{1}{(h_s-2\delta_{1,s})^2}-\dfrac{1}{D^2}}{\dfrac{1}{(h_0-2\delta_{1,0})^2}-\dfrac{1}{D^2}}, \qquad (15)$$

where $\delta_{1,0}$ is the displacement thickness of the boundary layer at the minimum contraction point.

Figures 7 and 8 show examples of the results of comparisons between theoretical expectations and measurements obtained for $h_0=0.96$ mm and $h_0=3.32$ mm as a function of the Reynolds number Re.

Figures 7 and 8 show the results of pressure measurements performed simultaneously on both sides of the model (P_2 and P_2'). At high Reynolds numbers strong asymmetry in the flow appears quite clearly from these results. This phenomenon, which is due to the Coanda effect, will be discussed in the next section.

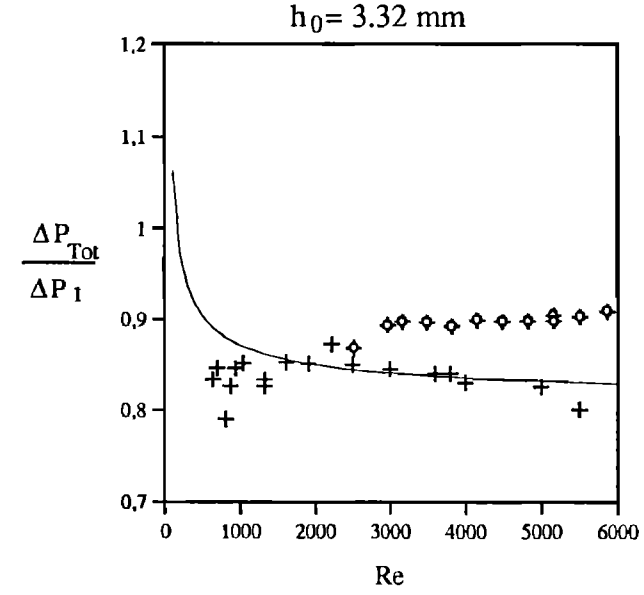

FIG. 8. Experimentally obtained and theoretically expected normalized pressure drop results for $h_0=3.32$ mm. The symbol + refers to P_2 measurements, -◇- to P_2' measurements.

Focusing on P_2 measurements only, we observe that for Reynolds numbers higher than about 2500 for $h_0=0.96$ mm and 2000 for $h_0=3.32$ mm (which are typical during phonation), the agreement between the theoretical model and the experimental results is fairly good. As the Reynolds number decreases below $\mathrm{Re}=10^3$, larger discrepancies (within 10%) appear between the theoretical model and the experimental results.

The same conclusions can be drawn for the different apertures tested: In most cases our theoretical model predicts the pressure differences within a few percent for high Reynolds numbers but for lower Reynolds numbers the agreement is less satisfying.

2. Unsteady-flow experiments

a. Relevance of the Coanda effect under unsteady conditions. Papers by Teager and Teager[22] and Kaiser[23] formally pointed out the importance of a possible asymmetry in the supraglottal flow, also known as the Coanda effect.[17] It is interesting to note that this effect was observed recently by means of full numerical simulation under steady conditions.[3] In performing measurements on both sides of the contraction in the model we indeed observed such an effect as shown in the preceding section (see Figs. 7 and 8). Further flow visualizations confirmed that this asymmetry in pressure measurements corresponded to an asymmetric jet flow.

As noted by Teager and Teager,[22] this asymmetry in the flow, which is usually not taken into account, would certainly be of great importance if implemented in a numerical model for the vocal cords. While there is no doubt that the Coanda effect occurs under steady-flow conditions, we do not expect it to occur under unsteady conditions. As an argument for this statement we present in Fig. 9 flow visualization performed under unsteady conditions such as an impulsively starting flow in the model. The experimental conditions were chosen to have a Strouhal number in the same order of magnitude as encountered in glottal flows [$\mathrm{Sr}=O(10^{-2})$].

As shown above, while in steady conditions a strong Coanda effect occurs, under unsteady conditions it appears clearly that the flow remains symmetric since the Coanda effect does not have time to establish itself. It is interesting to note that this conclusion is consistent with the results obtained by Iijima *et al.*[24] on the basis of a numerical solution of the unsteady Navier–Stokes equations.

b. Unsteady-flow measurements. The unsteady experimental conditions described in the preceding section also provide a good opportunity to evaluate the validity of the quasisteady theory under unsteady conditions. As previously stated, we expect, on account of the experimental conditions chosen, the unsteady effects to be in the same order of magnitude as those encountered during phonation.

Figure 10(a) presents the time-dependent pressure difference imposed on the model measured using a piezoelectric transducer (PCB type 116A). Bulk flow velocity was measured by means of hot-wire anemometry. The hot wire was carefully placed on the center line and at the throat of the

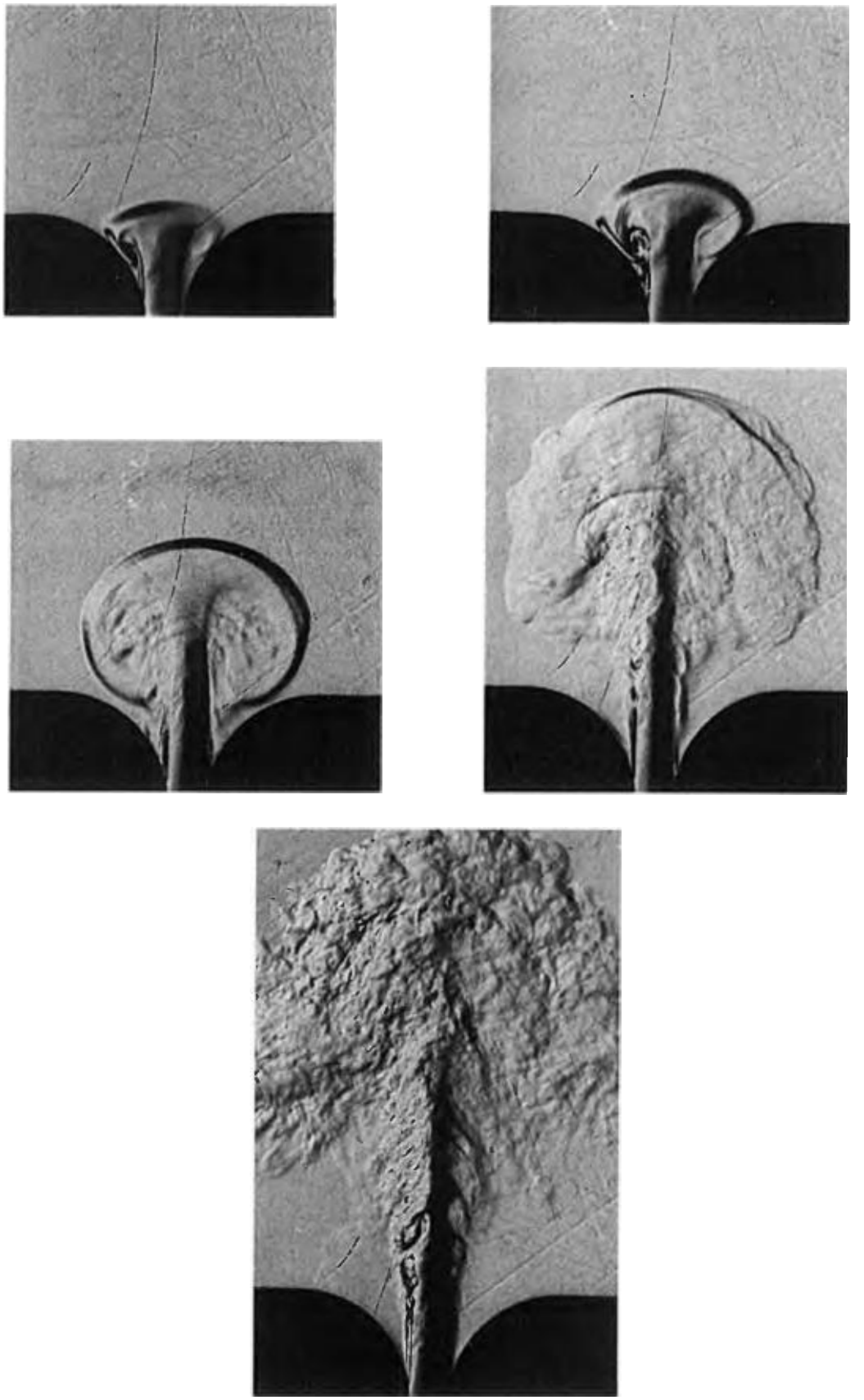

FIG. 9. Visualization of impulsively starting flow in the experimental model with $h_0 = 3.32$ mm. Flow visualization was obtained by a schlieren method. The refractive index was obtained by injecting CO_2 into the flow upstream of the model.

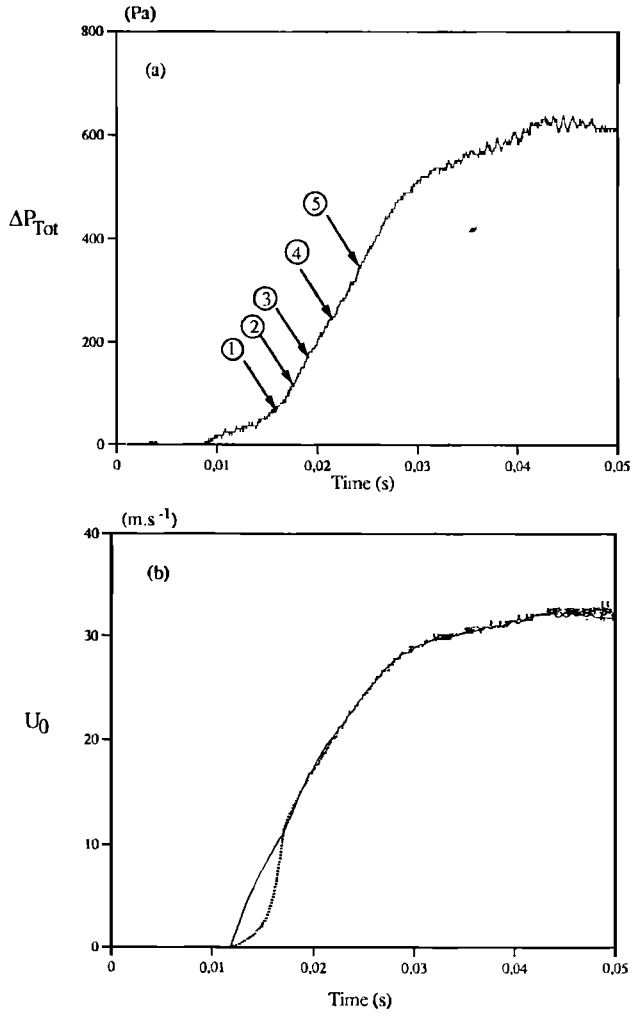

FIG. 10. Results for $h_0=3.32$ mm. (a) Time-dependent pressure difference imposed across the model during the impulsively starting flow experiments; corresponding pictures in Fig. 9 are indicated by numbers. (b) Corresponding measured flow velocity (dashed line) and theoretical expectation (solid line).

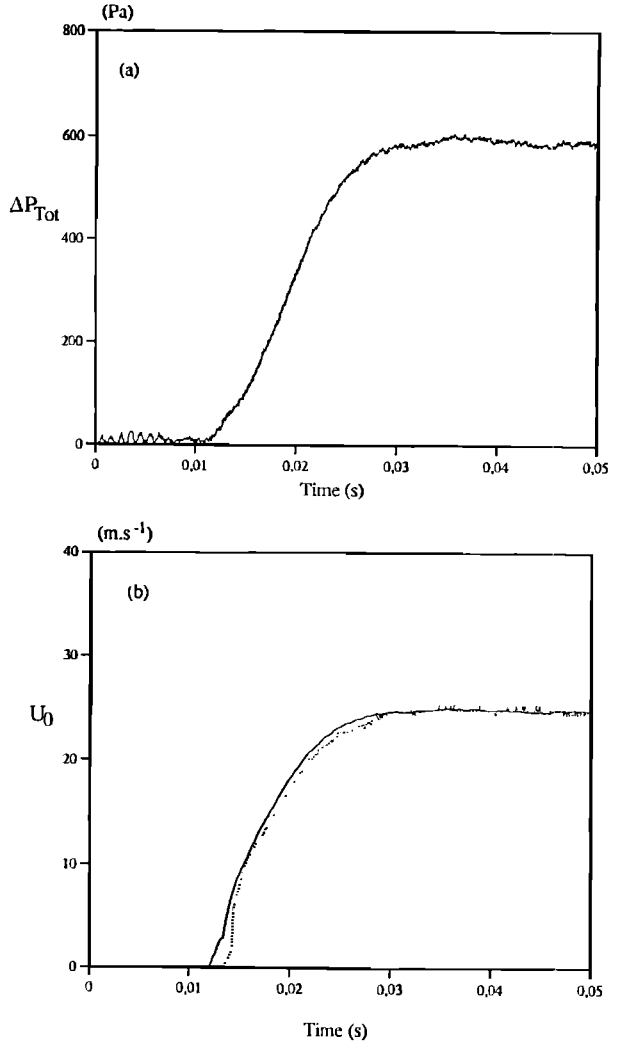

FIG. 11. Results for $h_0=0.96$ mm. (a) Time-dependent pressure difference imposed across the model during the impulsively starting flow experiments. (b) Corresponding measured flow velocity (dashed line) and theoretical expectation (solid line).

channel. Figure 10(b) presents the results of a comparison between the measured flow velocity and the theoretical expectation inferred from the pressure signal itself.

Figure 11(a) and 11(b) present another example of results obtained for a minimum aperture $h_0=0.96$ mm.

As can be seen in Figs. 10 and 11, the agreement between the quasisteady theory and the unsteady measurements appears to be quite acceptable. Significant differences occurred during the very first few milliseconds of the velocity signal, probably due to additional unsteady effects that are not taken into account in the simple theory presented here.

D. Conclusions and limits of the theory

With respect to the experiments described above, the theoretical flow model proposed here appears to be a quantitative improvement of the Ishizaka and Flanagan flow model. Limits of the theory appear for the prediction of pressure differences at low Reynolds numbers. It can be shown that a much more accurate flow prediction can be obtained for low Reynolds numbers (Re<300).[25] However, we do not think that such models are really needed. First, because the inaccuracies of the pressure prediction appear limited (10% at the most) and second, because they will mainly affect the pressure force description over a short period of time (namely the opening and the closing part of the vocal cords) during which we expect the inertial forces and the restoring forces due to the elasticity of the vocal cords to be predominant. Finally one should note that the flow model has been tested under simple experimental conditions. Thus the validity of the theory under conditions closer to phonation (pulsative flow, moving boundaries) is still to be tested. This constitutes future research.

III. APPLICATION TO THE TWO-MASS MODEL

In this section we will consider the application of the quasisteady model for flow separation derived in the preceding part to a numerical model of the vocal cords. Numerical models for the vocal cords are numerous and can be classified by considering the number of mechanical degrees of freedom they offer. Thus the models proposed in the litera-

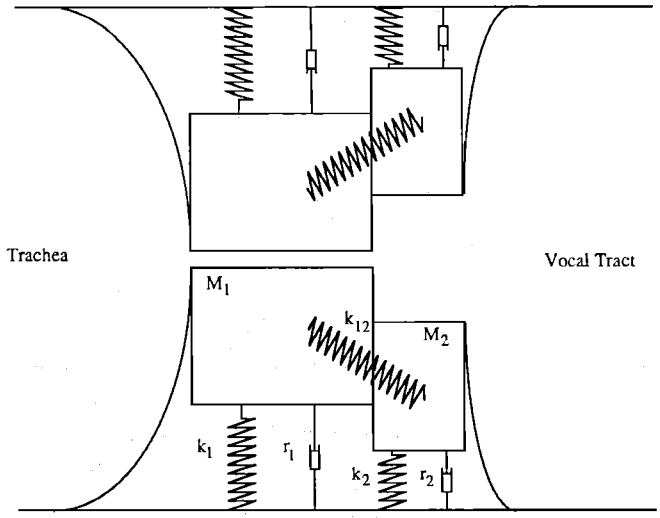

FIG. 12. Two-mass representation of the vocal cords.

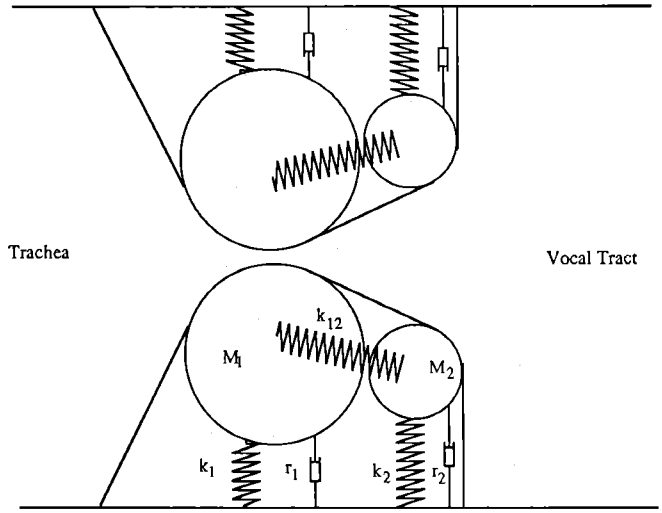

FIG. 13. Modified two-mass model.

ture vary from extremely simple ones, the simplest of which is the one-mass model of Flanagan and Landgraf[26] allowing only one degree of freedom, to very complex ones allowing up to 16 degrees of freedom[1] or even considering a continuous structure.[12] For reasons of simplicity, and also because it appears that it constitutes a reasonable compromise between complexity and efficiency, we will consider here an application to the two-mass model as proposed by Ishisaka and Flanagan.[8] In Ishizaka and Flanagan's representation each vocal cord is described as two rectangular masses coupled with springs (Fig. 12).

Such a model could also be understood as a model in which the movement of the vocal cords is described by two oscillation modes. Hence we could call it a two-mechanical-degrees-of-freedom model.

A. Description of the model

As can be easily understood from Fig. 12, it would not make much sense to introduce a quasisteady model for flow separation in the representation proposed by Ishizaka and Flanagan[8] since flow separation would always occur at the sharp edges in the model! For this reason, we propose a simple modification of the two-mass model in which the simple mechanical description of the vocal cords is retained, but for which this mechanical system drives a two-point parametric curve describing the shape of the vocal cords. The description we use is based on cylinders connected by tangent plates as shown in Fig. 13.[27,28]

1. Governing equations

The main differences, besides the shape, between our model and the classical rectangular description, recalled in Sec. I, can be listed as follows:

(1) We do not consider a vena contracta effect at the entrance of the glottal model,

(2) a quasisteady separation point is introduced in the model instead of a fixed separation point, and

(3) no pressure recovery is assumed at the outlet of the glottis.

The mechanical description is simplified by considering linear springs characteristics and by neglecting the pressure force exerted on the second mass. Finally, a modified description of the vocal cord closure will be introduced. This last point will be discussed in greater detail in Sec. III C. Table III summarizes the differences between the smooth and the rectangular model, while details of the governing equations and computation schemes can be found in appendixes A and B.

TABLE III. Comparison between the main assumptions and the equations governing the rectangular and the smooth two-mass models.

Rectangular Model	**Smooth Model**
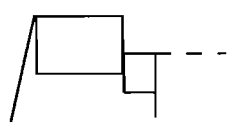	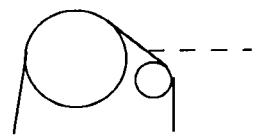
Fluid Mechanical description	
- Flow separation at the entrance of the glottis. (Vena contracta effect)	- Smooth, rounded and progressive entrance.
- Fixed separation point	- Quasi-steady model of separation :
- Quasi-steady pressure recovery model.	- Pressure recovery neglected
Mechanical description	
- Non linear spring model.	- Linear spring model
- Forces on both masses	- Force only on the first mass.
- Uniform pressure force :	- Non-uniform pressure force due to shape variations :
$\vec{F} = -Lg.h.P.d\vec{y}$	$\vec{F} = -Lg.\int_{Inlet}^{Separation} P(x).d\vec{S}$
- Abrupt closure of the vocal cords	- Deformation and contact model.

TABLE IV. Mechanical constants used for the computation of the rectangular and the smooth model.

	mass	$M_1=0.17$ g	
Mass 1	spring stiffness	opened condition	closed condition
	spring damping	$K_1=80$ N m^{-1}	$K_1=320$ N m^{-1}
		$r_1=2.33$ N s m^{-1}	$r_1=2.57\times10^{-1}$ N s m^{-1}
	mass	$M_2=0.03$ g	
Mass 2	spring stiffness	opened condition	closed condition
	spring damping	$K_2=8$ N m^{-1}	$K_2=32$ N m^{-1}
		$r_2=1.86\times10^{-2}$ N s m^{-1}	$r_2=4.96\times10^{-2}$ N s m^{-1}
Coupling spring	spring stiffness	$K_{12}=55$ N m^{-1}	

All these modifications are of a different nature and their consequences are difficult to evaluate *a priori*. For this reason, we will now present a detailed numerical study focusing in particular on the influence of each modification.

B. Simulation results

We will present a systematic comparison between the rectangular and the smooth model for the vocal cords. The mechanical constants we chose are presented in Table IV; they were the same for both models.

For the rectangular model, nonlinear spring stiffnesses were considered. We used the nonlinear constants proposed by Ishizaka and Flanagan[8] ($\eta=100$ during opened conditions and $\eta=500$ during closed conditions). The effective glottal thickness was chosen to be 0.3 cm for both models (mass 1 thickness was 0.25 cm, mass 2 thickness 0.05 cm). The initial aperture of the glottis (neutral position) was chosen to be 0.0014 mm.

Finally, the subglottic pressure signal was described as a smoothly increasing signal whose maximum value of 980 Pa (10 cm H_2O) is reached after 10 ms.

As a basis for comparison, we will present in the next section results obtained for the volume velocity U_g, as well as for its time derivative dU_g/dt, because the latter signal constitutes the excitation signal for the vocal tract.

1. Curvature effects

In Fig. 14 we present results obtained with the rectangular model and a version of the smooth model for which the separation was imposed to occur at the end of the model and was not allowed to move.

A very important quantitative difference is observed in the predicted volume velocities: The smooth model predicts values that are much higher than those expected on the basis of the rectangular model. These differences can of course be explained by the different fluid mechanical description used, especially when not considering the strong losses due to a vena-contracta effect. Indeed, these losses do not only reduce the predicted flow velocity through the Bernoulli equation but also reduce the pressure forces exerted upon the masses. As a consequence, the apertures computed with the classical model are smaller than those obtained using the smooth model and contribute again to reduce the flow velocity. This statement can easily be verified by suppressing the vena-contracta factor in the rectangular model. We then find peak flows of the order of 750 cm^3 s^{-1} which are close to those obtained with the smooth model. Moreover, both models oscillate with comparable fundamental frequency (162 Hz in the rectangular model versus 160 Hz in the smooth model). Concerning the glottal waveforms, the differences are limited. In particular, the typical discontinuities in U_g at closure as well as the unrealistic negative peak flows in dU_g/dt are observed for both models.

2. Flow-separation effects

We will now present results obtained with our model with allowance for a quasisteady separation of the flow. As appears in Fig. 15, the consequences are qualitatively and quantitatively significant.

In Fig. 15, the ratio between the jet diameter h_s (glottal aperture at the flow-separation point) and the aperture at the outlet of the glottis h_2 is also presented. As this quantity was imposed to unity in Ishizaka and Flanagan's[8] two-mass model, it is no longer a constant in the present model. As a matter of fact, we see from Fig. 15(c) that the flow-separation position is first moving upstream of the glottis in the beginning of the closing phase. During the last part of the closing phase (prior to the closure) this motion is inverted and the separation point is then moving downstream. By comparison with Fig. 14, an important decrease of the fundamental frequency (down to 135 Hz) is observed. Concerning the waveforms, the main differences of course occur during the closing phase, when the glottis presents a diverging shape in which flow separation can take place. In particular, the strong negative peaks in the time derivative of the volume velocity are much less pronounced in the smooth model. This result can be explained with respect to Fig. 15(c) since the major differences with the Ishizaka and Flanagan[18] model are indeed occurring during this part of the closing phase.

C. Other improvements: Closure of the vocal cords

1. Deformation of the vocal cords during contact

Modeling of the closure of the vocal cords is also important with respect to the quality of the generated speech signals. Abrupt closure of the vocal cords can lead not only to undesirable generation of higher harmonics but also to an inaccurate description of the closing and the closed portion of the glottal signals. In the following we propose a more realistic description of the vocal cords collision taking into account the elastic deformation of the tissues. We thus consider that during closure of the vocal cords a certain amount

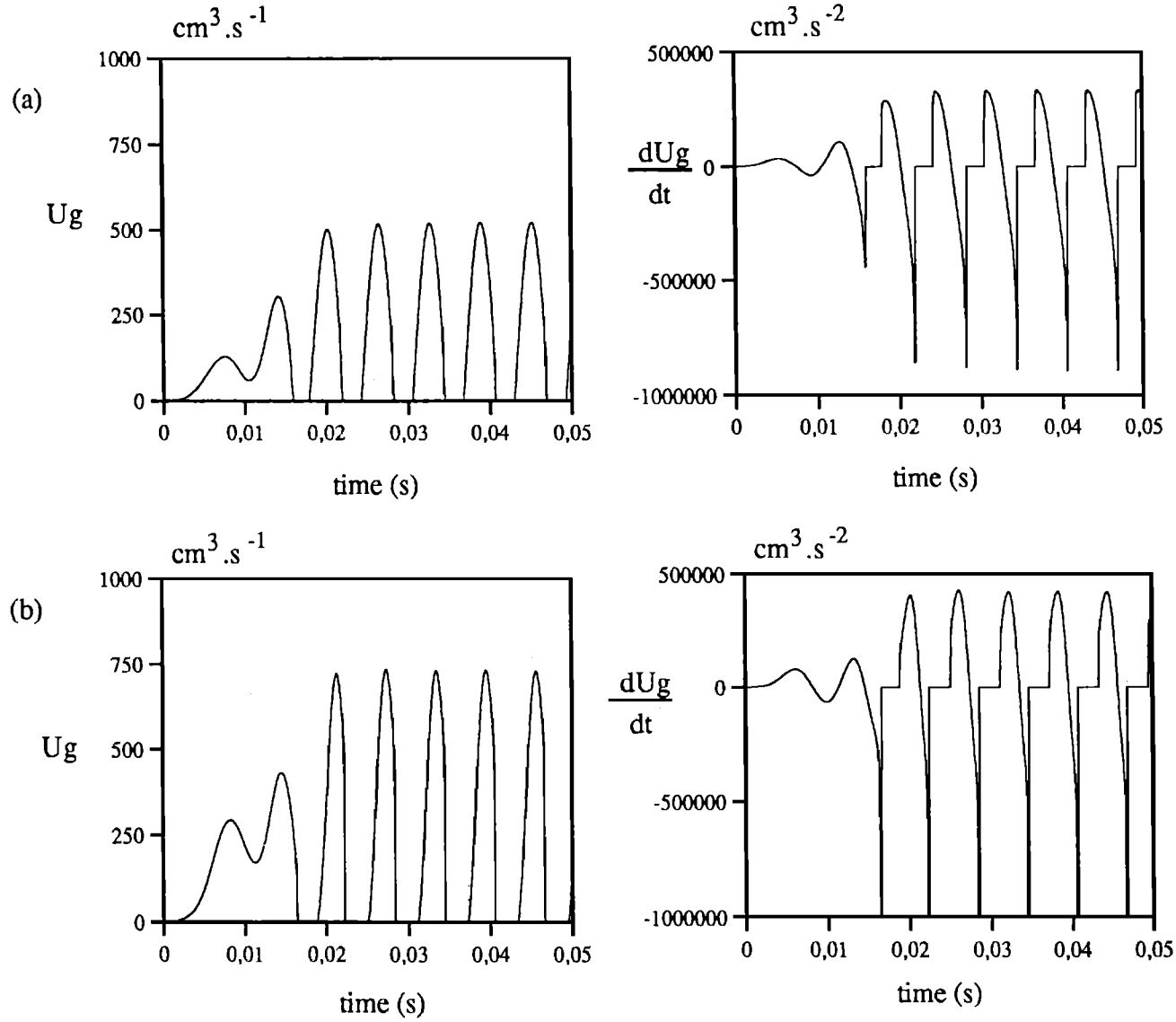

FIG. 14. Computed volume velocity and corresponding time derivative as a function of time, obtained for (a) the rectangular two-mass model and (b) the smooth model with a fixed separation point.

of air is expelled due to the deformation of the tissues. This additional flow U_g^*, although very weak, is of importance since it prevents discontinuities in the glottal waveform, as shown Fig. 16.

An important consequence for the quality of the signals is that the resulting spectrum is much less rich in high harmonics which in the rectangular model yield the typical "computer accent."

2. Vocal cord contact and glottis closure

It is generally assumed that contact of the vocal cords implies a complete closure of the glottis. In fact, high-speed recordings of the human vocal cords during phonation as well as *in vivo* measurements[29] reveal that the vocal cords gradually collide from the lateral sides to the middle part or that in some cases, during breathy voicing for instance, the glottis never closes completely. As a result, there is still a certain amount of air which is allowed to pass the glottis while the vocal folds are already in contact with each other.

To model such an effect in a simple way, we propose to consider that there is a certain time gap between the contact of the vocal cords and the effective closure of the glottis. Accordingly, we introduce a certain critical aperture at which the vocal cords are considered to be mechanically in contact while the glottis remains opened until a second critical position (aperture zero) is reached. In the example shown in Fig. 17 the critical aperture was chosen to be $h_c = 0.2$ mm.

It is interesting to note that a wider critical aperture can lead to a situation in which the glottis is never completely closed. This then constitutes an alternative description of the "leaky glottis" discussed by Cranen.[29]

D. Comparison with real speech signals

So far we have presented successive modifications of a simple numerical model for the vocal cords and have evaluated the consequences of these modifications through comparison with a classical description. Of course, without considering the coupling of the numerical model with a model for the vocal tract, the effective impact of our model on

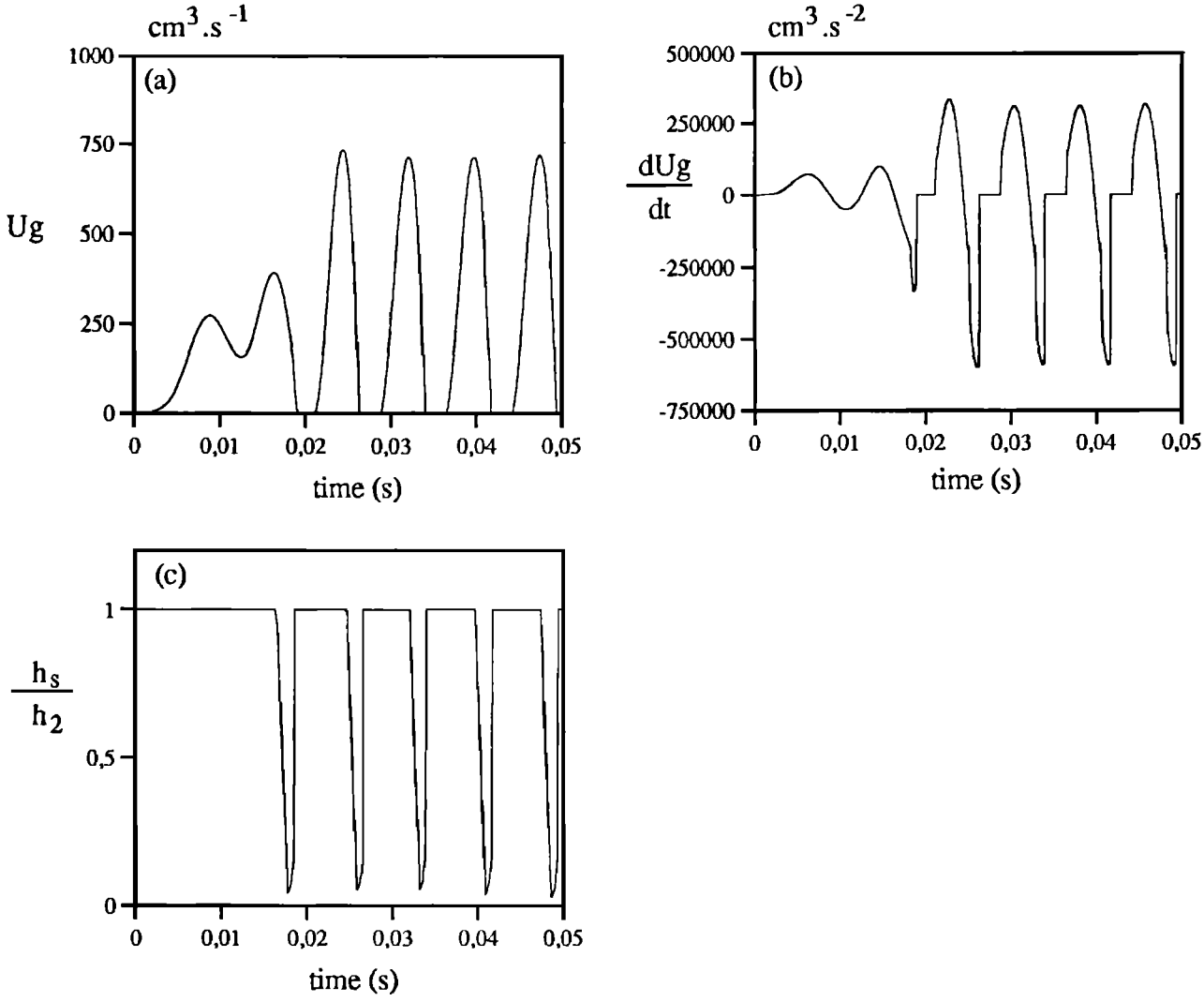

FIG. 15. (a) Computed volume velocity, (b) corresponding time derivative, (c) and ratio between the jet diameter h_s to the glottal outlet h_2 as a function of time, obtained for the smooth model with a quasisteady-flow separation.

synthetic speech remains difficult to evaluate in greater detail. However, qualitative insight can be obtained by comparing simulation results with the glottal signals derived from inverse filtering obtained by Eggen.[9] In Fig. 18 we present the results of such a comparison in which the inverse filtered glottal signal was measured on a male speaker (normal voice) and the synthetic signal was obtained using our complete numerical program including the vocal cords collision model described in Sec. III C. Simulation parameters were chosen in order to have a fundamental frequency comparable to the inverse filtered data. The spring stiffnesses were $K_1=60$ N m^{-1}, $K_2=8$ N m^{-1}, and $K_{12}=55$ N m^{-1}, the maximum subglottic pressure was 588 Pa (6 cm H_2O), the critical aperture h_c was chosen to be 0.11 mm, and other parameters were kept the same as in the previous sections.

Although the comparison presented enhances some differences at particular points, the global shapes present some similarities. This qualitative example tends to show that the modifications proposed here can lead to signals that are quite different from those obtained with Ishizaka and Flanagan's[8] model but not unrealistic when compared with real speech.

IV. CONCLUSION

In this paper we have discussed the relevance of the currently used description of the air flow through the vocal cords. We have shown that many effects, such as flow separation at the entrance of the glottis, flow reattachment at the glottal outlet, and asymmetry in the flow due to the Coanda effect discussed in the literature or used in numerical models, do not appear to be relevant in the case of phonation. We then presented a revised quasisteady theoretical flow model, focusing in particular on the description of flow separation in the diverging channel formed by the smooth boundaries of the vocal cords. The flow-separation prediction model we proposed was kept simple enough for a numerical program for speech production. This theory was found to be in reasonable agreement with steady- as well as with unsteady-flow measurements, which goes to prove that the quasisteady assumption is a reasonable one in phonation conditions.

The second part of this paper was dedicated to a study of the consequences of the revised theory when applied to the

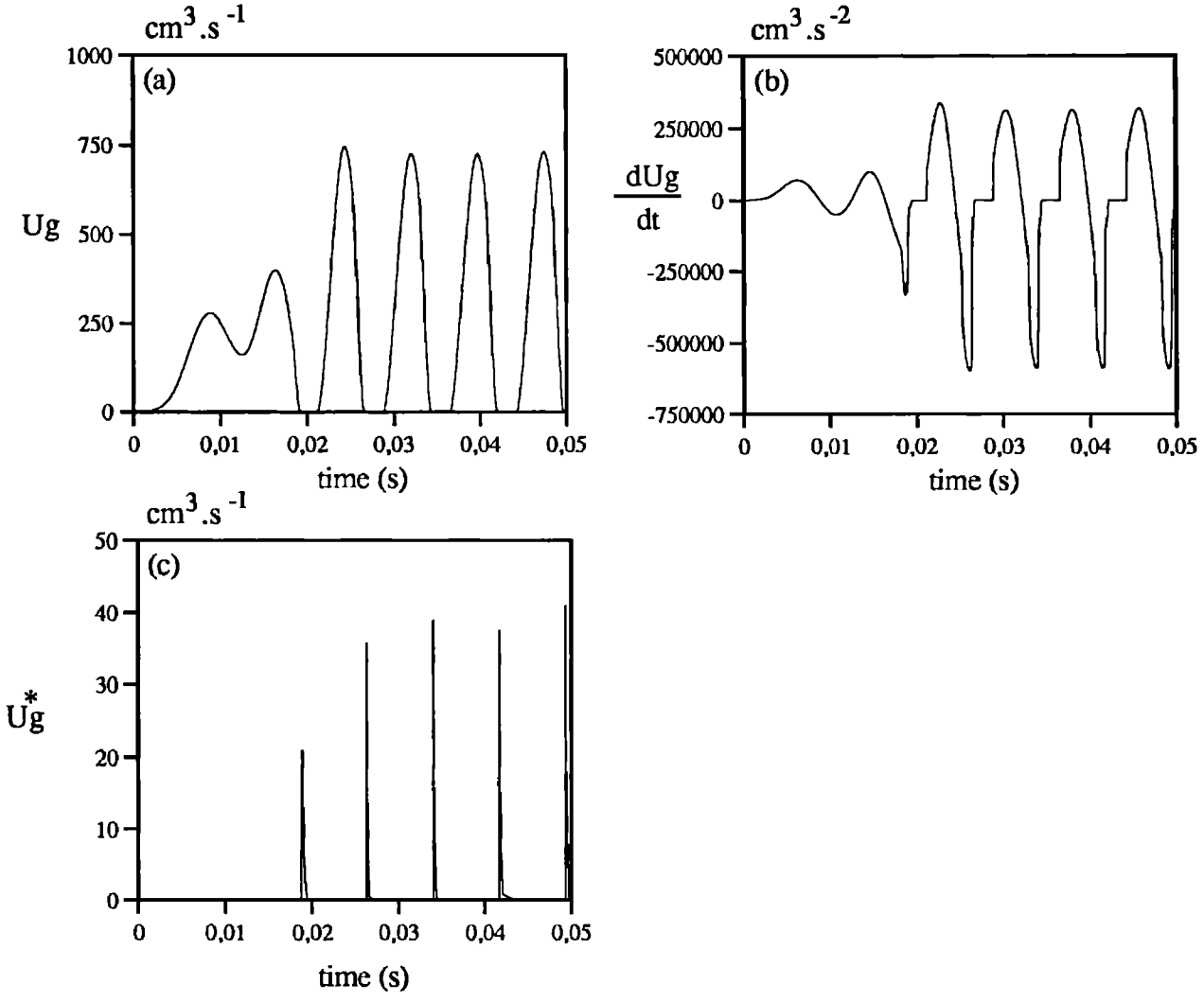

FIG. 16. (a) Computed volume velocity and (b) corresponding time derivative obtained using a vocal cords deformation model at closure. The additional volume velocity due to the vocal cords deformation is presented in (c).

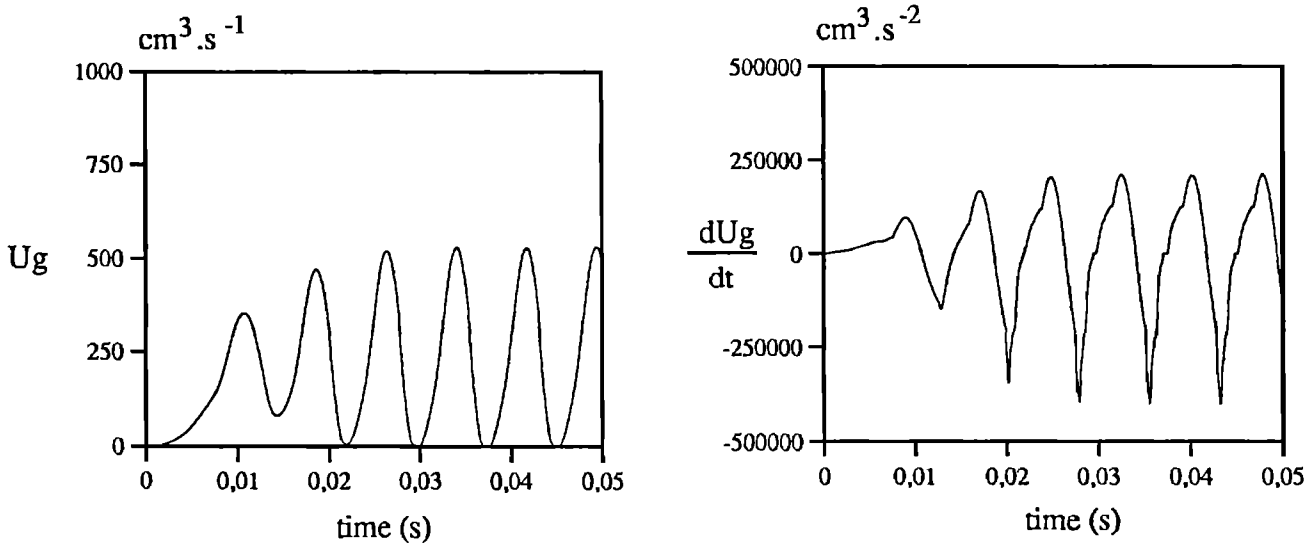

FIG. 17. Computed volume velocity and corresponding time derivative obtained using a delayed closure model.

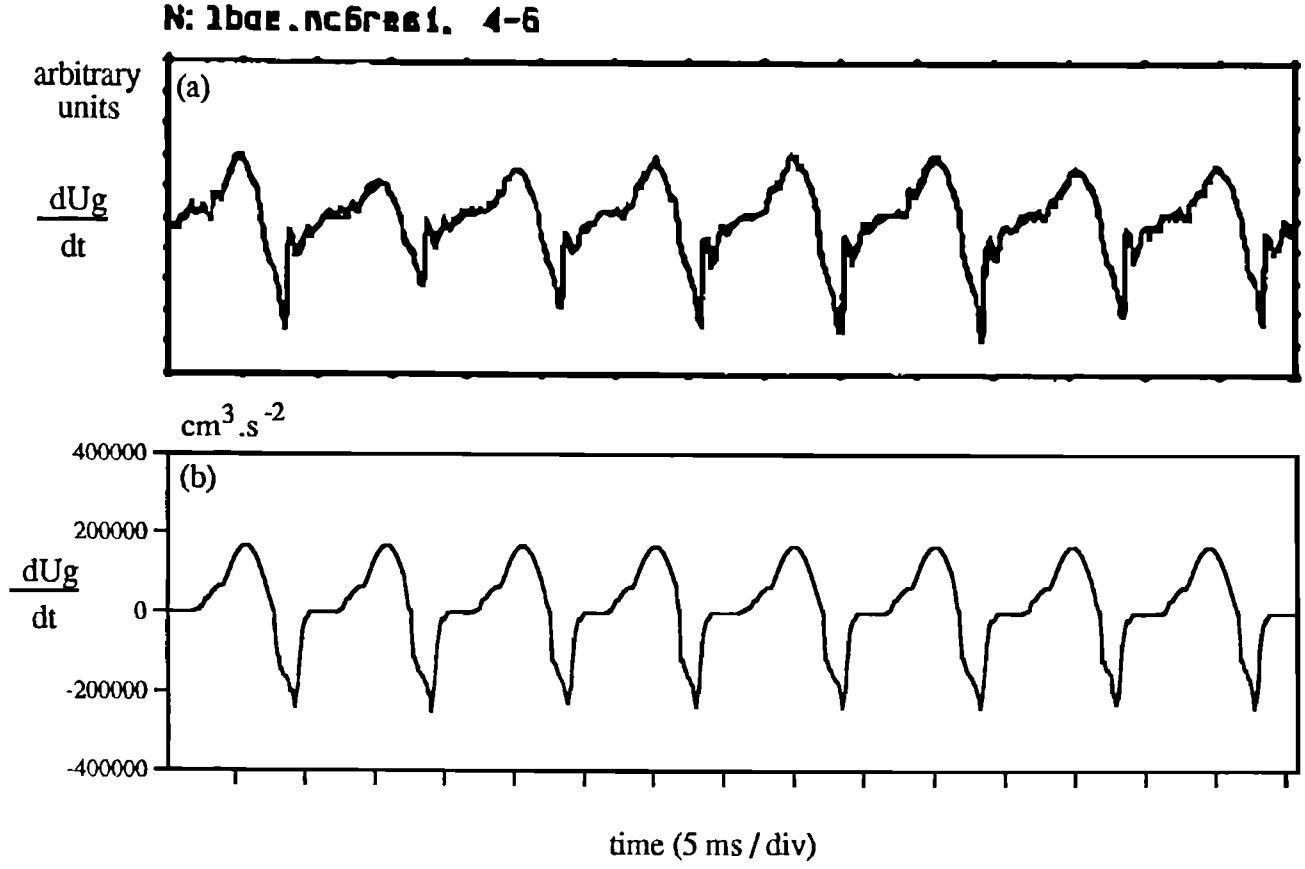

FIG. 18. Comparison of glottal volume velocity time derivatives obtained by means of (a) inverse filtering performed on real speech and (b) numerical simulation using the smooth model.

numerical simulation of voiced sounds. Although the theory we proposed could be implemented in any existing mechanical model, we chose for the sake of simplicity the most simple representation of the vocal cords: the two-mass model. The two-mass model proposed, although mechanically equivalent to that proposed by Ishizaka and Flanagan,[8] presents some important differences from a fluid mechanical point of view but also in terms of the general geometry. Among the modifications proposed, the moving flow-separation point appears to be the most significant, affecting the resulting glottal signals both qualitatively and quantitatively.

A numerical model having a smooth shape allows the introduction of a more realistic flow model and also allows simple modifications to describe physiological phenomena that occur during closure of the vocal cords. In particular, the simple models were presented in order to describe the deformation of the vocal cords; nonuniform closure of the glottis already seems to lead to more realistic signals. It appears that these modifications can be at least as important as the introduction of a moving separation point to mimic the measured glottal waveforms reported in the literature.

ACKNOWLEDGMENTS

This work was financially supported by Grant No. SWEd/4 of the Netherlands Foundation for Fundamental Research on Matter (FOM). Initial part of the work was also granted by the Institute for Perception Research (IPO), the Ambassade de France in The Hague, and the Technical University of Eindhoven. The authors wish to thank Louis Ten Bosch and Barry Eggen of the Institute for Perception Research, P. Badin and Eric Castelli of the Institut de la Communication Parlée, and René Reneerkens, Stefan Belfroid, Meline van't Hof, and Hélène Baillet for their participation in this work and their helpful discussions.

APPENDIX A: SMOOTH MODEL EQUATIONS

1. Fluid flow formulation

The general fluid flow model is based on the following coupled equations:

$$\Delta P_{\text{Tot}} = \Delta P_{\text{Bernoulli}} + \Delta P_{\text{viscous}}, \tag{A1}$$

$$L_g \frac{\partial h(x)}{\partial t} + \frac{\partial U_g}{\partial x} = 0, \tag{A2}$$

where the second equation is expressing the conservation of mass.

Bernoulli term formulation. Let us first consider the unsteady Bernoulli theorem applied between two regions 1 and 2 of the flow:

$$\rho \frac{\partial \varphi_1}{\partial t} + \frac{1}{2}\rho v_1^2 + P_1 = \rho \frac{\partial \varphi_2}{\partial t} + \frac{1}{2}\rho v_2^2 + P_2, \tag{A3}$$

where P_1, v_1 (P_2 and v_2, respectively) are the pressure and the velocity in region 1 (and in region 2, respectively), and where the potential φ is defined as

$$\varphi = \int \frac{U_g}{L_g h(x)}\, dx. \tag{A4}$$

When applied to the smooth model of the vocal cords depicted in Fig. 13, and allowance is made for the fact that the diameter of the trachea is much larger than the glottal aperture, the pressure difference between the sub- and supraglottal regions is found to be

$$\Delta P_{\text{Bernoulli}} = P_{\text{Sub}} - P_{vt} = \rho \frac{\partial}{\partial t}\left(\int_{x_{\text{sub}}}^{x_s} \frac{U_g}{L_g h(x)}\, dx \right) + \frac{1}{2}\rho \frac{U_g^2}{L_g^2}\left(\frac{1}{h(x_s)^2} \right), \tag{A5}$$

where x_s is the abscissa of the separation point and x_{sub} the abscissa of the entrance of the glottis.

Viscous losses. As already stated, formula (A3) is only valid when viscous effects can be neglected. In the special case for which the glottis is closing or opening the apertures involved can become so narrow that this assumption is no longer valid and viscous effects can even become predominant. In such a case the momentum equation reduces to the following form, on the assumption of a fully developed Poiseuille flow:

$$\frac{dP}{dx} = -\frac{12\mu}{L_g h(x)^3} U_g. \tag{A6}$$

If we apply formula (A6) between the sub- and supraglottal regions, we find

$$\Delta P_{\text{viscous}} = \frac{12\mu}{L_g} U_g \int_{x_{\text{sub}}}^{x_s} \frac{1}{h(x)^3}\, dx. \tag{A7}$$

Calculation of the separation point. For a given geometry of the vocal cords [$h(x)$ known] and a given main flow velocity U_0 (Re known), the function $\lambda(x)$ can be easily computed for every x using the formula

$$\lambda(x) = -\delta_2^2(x)\,\text{Re}\, \frac{1}{[h(x) - 2\delta_1(x)]^2} \times \left(\frac{dh(x)}{dx} - 2\frac{d\delta_1(x)}{dx} \right), \tag{A8}$$

and

$$\delta_2^2(x) = \delta_{2,0}^2(x) + K^2 \frac{1}{\text{Re}} [h(x) - 2\delta_1(x)]x. \tag{A9}$$

Flow separation is predicted to occur for $x = x_s$ such that

$$\lambda(x_s) = -0.0992. \tag{A10}$$

2. Mechanical formulation

Let y_1 and y_2 be the instantaneous displacement of masses M_1 and M_2. The fundamental principle of mechanics gives

$$M_1 \frac{d^2y_1}{dt^2} + r_1 \frac{dy_1}{dt} + K_1 y_1 + K_{12}(y_1 - y_2) = F_1, \tag{A11}$$

$$M_2 \frac{d^2y_2}{dt^2} + r_2 \frac{dy_2}{dt} + K_2 y_2 + K_{12}(y_2 - y_1) = F_2, \tag{A12}$$

where $F1$ and $F2$ are the modulus of forces exerted by the flow on masses 1 and 2 in the y direction. For the sake of simplicity, we assumed that no fluid mechanical force is exerted on mass 2($F2 = 0$). In other words, we consider the second mass to be totally driven by the first one.

$F1$ can be calculated in a similar way as presented in Sec. 1, by introducing a Poiseuille term as a correction to the Bernoulli formula:

$$F_1 = -\int_{\text{mass 1}} \left(P_{\text{sub}} - \frac{\rho}{L_g} \int_{x_{\text{sub}}}^{x} \frac{1}{h(\zeta)}\, d\zeta \frac{dU_g}{dt} - \frac{1}{2}\rho \frac{U_g^2}{L_g^2 h^2(x)} - \frac{12\mu}{L_g} U_g \int_{x_{\text{sub}}}^{x} \frac{1}{h^3(\zeta)}\, d\zeta \right) dS, \tag{A13}$$

APPENDIX B: NUMERICAL RESOLUTION

The general numerical scheme for a given time step i is summarized in Fig. B1. The two tests on $h_1(i)$ [or $h_2(i)$] refer to the collision model described in Sec. III C 2 a. Distinction between the vocal cord contact and the glottal clo-

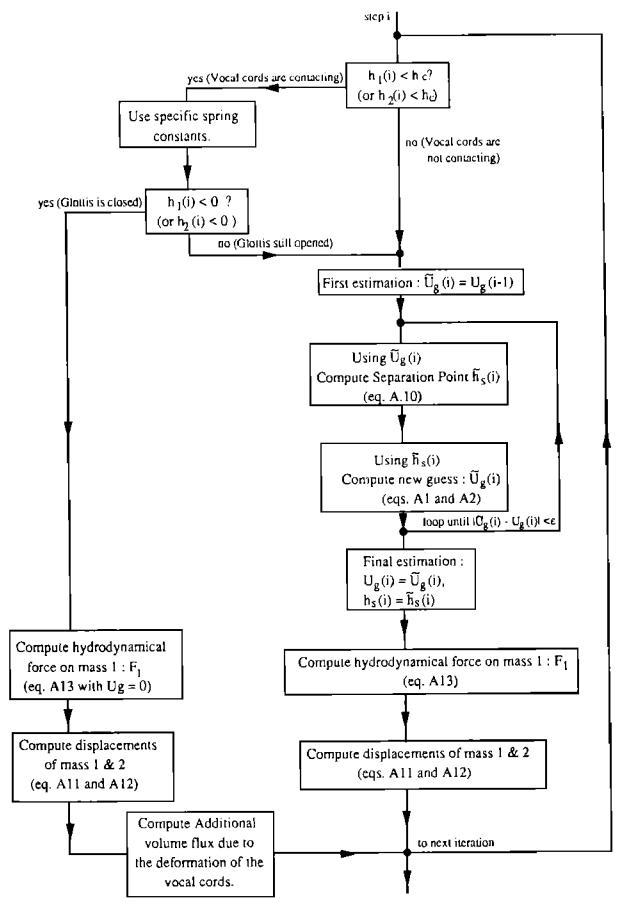

FIG. B1. Flow chart of the numerical resolution for the modified two-mass model.

sure is made by using the critical aperture h_c. In the case where the glottis is opened, the volume velocity $U_g(i)$ is then found by an iterative procedure. At each step within the loop equations (A1) and (A2) are simultaneously solved using a finite differences technique. A typical convergence criterion ϵ was chosen to be $\epsilon=10^{-6}$. Lastly, the mechanics of the model is computed using a finite differences scheme and in the case of a closed glottis, allowance is made for additional air flow due to the deformation of the vocal cords.

[1] I. R. Titze, "Normal modes in vocal cord tissues," J. Acoust. Soc. Am. **57**, 736–744 (1975).

[2] R. C. Scherer, "Physiology of phonation: A review of basic mechanics," in *Phonosurgery: Assessment and Surgical Management of Voice Disorders*, edited by C. N. Ford and D. M. Bless (Raven, New York, 1991), pp. 77–93.

[3] F. Alipour, "Airflow instabilities and asymmetries in the narrow glottal constriction," paper presented at 3rd Seminar on Speech Production, New Haven (unpublished).

[4] J. Liljencrants, "Numerical simulations of glottal flow," in *Vocal Fold Physiology*, edited by J. Gauffin and B. Hammerberg (Singular, San Diego, CA, 1989), pp. 99–104.

[5] R. C. Scherer, I. R. Titze, and J. F. Curtis, "Pressure-flow relationship in two models of the larynx having rectangular glottal shapes," J. Acoust. Soc. Am. **73**, 668–676 (1983).

[6] J. Gauffin, N. Binh, T. V. Ananthapadmanabha, and G. Fant, "Glottal geometry and volume velocity waveform," in *Vocal Fold Physiology*, edited by D. M. Bless and J. M. Abbs (College Hill, San Diego, CA, 1983), pp. 194–201.

[7] B. Cranen and L. Boves, "Pressure measurements during speech production using miniature pressure transducers: Impact on models for speech production," J. Acoust. Soc. Am. **77**, 1543–1551 (1985).

[8] K. Ishizaka and J. L. Flanagan, "Synthesis of voiced sounds from a two-mass model of the vocal cords," Bell Syst. Tech. J. **51**, 1233–1267 (1972).

[9] J. H. Eggen, "On the quality of synthetic speech evaluation and improvements," Ph.D. thesis, Techn. Univ. Eindhoven, The Netherlands (1992).

[10] M. Hirano, "Structure and vibratory behaviour of the vocal folds," in *Dynamic aspects of Speech Production*, edited by M. Sawashima and F. S. Cooper (University of Tokyo, Tokyo, 1977). pp. 13–27.

[11] M. Hirano, S. Kurita, and T. Nakashima, "Growth, development and aging of human vocal folds," in *Vocal Fold Physiology*, edited by D. M. Bless and J. H. Abbs (College Hill, San Diego, CA 1983), pp. 22–43.

[12] R. Descout, J. Y. Auloge, and B. Guérin, "A continuous model of the vocal source," Proc. ICA-SSP, pp. 61–64 (1977).

[13] J. van den Berg, J. T. Zantema, and P. Doornenbal, "On the air resistance and the Bernoulli effect of the human larynx," J. Acoust. Soc. Am. **29**, 626–631 (1957).

[14] J. A. Miller, J. C. Pereira, and D. W. Thomas, "Fluid flow through the larynx channel," J. Sound Vib. **121**, 277–290 (1988).

[15] R. D. Blevins, *Applied Fluid Dynamic Handbook* (Van Nostrand Reinhold, New York, 1984).

[16] A. Hirschberg, "Some fluid dynamical aspects of speech," Bull. Commun. Parlée, **2**, 1–30 (1992).

[17] D. J. Tritton, *Physical Fluid Dynamics* (Clarendon, Oxford, 1988) 2nd ed.

[18] H. Schlichting *Boundary Layer Theory*, 6th ed. (MacGraw-Hill, New York, 1968), 6th ed.

[19] N. Curle, *The Laminar Boundary Layer Equations* (Oxford U. P., London, 1962) 1st ed.

[20] *Laminar Boundary Layers*, edited by L. Rosenhead (Dover, New York, 1963).

[21] J. Cousteix, *Aerodynamique, Couche Limite Laminaire* (Cepadues, Toulouse, 1988).

[22] H. M. Teager, and S. M. Teager, "Active fluid dynamics voice production, or there is a unicorn in the garden," in *Vocal Fold Physiology: Biomechanics, Acoustics and Phonatory Control*, edited by I. R. Titze and R. S. Scherer (The Denver Center for Performing Arts, Denver, CO, 1985), pp. 387–394.

[23] J. F. Kaiser, "Some observations on vocal tract operation from a fluid flow point of view," in *Vocal Fold Physiology: Biomechanics, Acoustics and Phonatory Control*, edited by I. R. Titze and R. S. Scherer (The Denver Center for Performing Arts, Denver, CO, 1983), pp. 358–386.

[24] H. Iijima, N. Miki, and N. Nagai, "Glottal impedance based on a finite element analysis of two-dimensional unsteady viscous flow in a static glottis," IEEE Trans. Signal Process. **40**, 2125–2135 (1992).

[25] T. J. Pedley, *The Fluid Mechanics of Large Blood Vessels* (Cambridge U. P., Cambridge, 1980).

[26] J. L. Flanagan and L. L. Landgraf, "Self-oscillating source for vocal-tract synthesizers," Proc. IEEE-AFCRL Symposium on Speech Commun. and Process., Boston, MA, 57–64 (1967).

[27] X. Pelorson, "A study of the two-mass model for the vocal cords from a fluid dynamical point of view," IPO Rep. No. 873.

[28] X. Pelorson, A. Hirschberg, and Y. Auregan, "Modified two-mass model for the vocal cords," J. Acoust. Soc. Am. **93**, 2417(A) (1993).

[29] L. I. J. Cranen, "The acoustic impedance of the glottis, measurements and modelling," Ph.D. thesis, University of Nijmegen, The Netherlands (1987).